Parametric scattering processes in photorefractive periodically poled lithium niobate

Evgueny Podivilov and Boris Sturman

Institute of Automation and Electrometry of RAS, Koptyug Avenue 1, 630090, Novosibirsk, Russia

Mikhail Goul'kov and Serguey Odoulov

Institute of Physics, National Academy of Sciences, 03650, Kiev-39, Ukraine

Gabriel Calvo, Fernando Agulló-López, and Mersedes Carrascosa

Universidad Autónoma de Madrid, E-28049 Madrid, Spain

We present an analysis of photorefractive properties of bulk periodically poled lithium niobate. The results obtained are applied to description and interpretation of phase-matched four-wave processes found recently in this novel nonlinear material. These processes manifest themselves in rings, lines, and dots of light-induced scattering that are essentially different from those known for single-domain crystals. We conclude that periodically poled lithium niobate is a new nonlinear material promising for various photorefractive applications. © 2002 Optical Society of America

OCIS codes: 160.5320, 190.5330.

1. INTRODUCTION

Periodically poled lithium niobate (PPLN) and other periodically poled ferroelectrics have attracted considerable research interest in recent years because of the prospects for quasi-phase-matched frequency conversion[1–4] and also as photonic-bandgap materials.[5] This interest is largely due to the progress in fabrication of high-quality periodically poled ferroelectrics. Photorefraction was regarded as a harmful effect at this stage. It was expected to be avoided by the use of undoped (or specially doped) crystals and also because of the suppression of the photorefractive response in the system of periodically alternating domains.[6]

In 1995, it was found experimentally in undoped planar PPLN wave guides that the photorefractive nonlinearity manifests itself at high intensities in an unusual light-induced scattering.[7] Some features of this phenomenon were interpreted in Ref. 8 on the basis of the conventional photorefractive concepts.

In 1997, it was predicted[9] that periodically poled ferroelectrics can be considered as new photorefractive materials combining suppression of large-scale variations of the refractive index (optical damage) with a strong nonlinear response at high spatial frequencies. This feature allows one to avoid deterioration of coherent light beams and, at the same time, provides their efficient nonlinear coupling. A possibility for occurrence in bulk PPLN samples of new nonlinear-wave processes, impossible in single-domain crystals, was also indicated in Ref. 9. Furthermore, it was found that the photorefractive properties of PPLN are rather insensitive to spatial fluctuations of the periodic domain structure.[10]

Fabrication of bulk Fe- and Y-doped PPLN samples en-abled recently, in 2000, direct experimental studies of the photorefractive properties of this nonlinear material.[11] The results of these studies have given solid evidence of coexistence of strong grating recording at sufficiently high spatial frequencies with a strong suppression of the optical damage. Further experiments[12] revealed a wide variety of nonlinear-wave processes in PPLN:Y:Fe, from those known for single-domain crystals[13] to essentially new ones, which are caused by the periodicity of the domain structure.

Most of the nonlinear processes in PPLN:Y:Fe manifest themselves as angular light singularities: rings, lines, and dots of light-induced scattering. The positions of the singularities are defined by proper phase-matching conditions. These conditions may include not only the wave vectors of the interacting waves but also the grating vector of the periodic domain structure.

It is important that the nonlinear properties of PPLN:Y:Fe (as those of bulk $LiNbO_3$ crystals) are polarization sensitive. They involve not only a spatial modulation of light intensity but also modulation of the polarization state. This property is due to the dominating photovoltaic mechanism of charge separation and tensorial properties of the photovoltaic effect.[14] The wealth of possibilities for charge separation in $LiNbO_3$ leads, in combination with the effect of periodicity, to a wide variety of strong light singularities in PPLN:Y:Fe.

The purpose of this paper is to analyze the properties of the photorefractive response of PPLN, including orientational and polarization dependences, to apply the results obtained for description of the most important four-wave processes, and to compare theoretical predictions with available experimental data.

The paper is organized as follows: In Section 2 we formulate a theoretical model of the transport and nonlinear optical phenomena in PPLN. In Section 3, on the basis of phase-matching conditions for light wave vectors, we analyze the general features of scattering processes and formulate some goals for the subsequent quantitative considerations. Section 4 is devoted to the photorefractive response of PPLN for the drift, diffusion, and photovoltaic mechanisms of charge separation. We assume here an arbitrary orientation of the light wave vectors, the grating vector of the periodic PPLN structure, and the direction of the light-induced electric current. Our analysis includes calculations of the amplitudes of the Fourier harmonics of the light-induced change of the optical permittivity and consideration of a number of particular cases. In Section 5 we apply the results of Sections 3 and 4 to description of a number of light rings, lines, and dots detected in experiment. Conclusions are drawn in Section 6.

2. BASIC MODEL

We assume in accordance with experiment[11,12] that PPLN structure consists of alternating plus and minus domains, as shown in Fig. 1. The unit polar vector **c** characterizing the direction of spontaneous polarization is parallel to the domain walls. The structure is symmetric, i.e., the positive and negative domains have the same size, $x_{\pm} = x_0$; the period of the structure is therefore $2x_0$. This case is shown to be optimum for photorefractive applications.[9] The x axis is chosen to be perpendicular to the domain walls, and the z axis is parallel to the vector **c**. Next we define the grating vector of the periodic domain structure, $\mathbf{G} = \pi\mathbf{n}_x/x_0$, where $\mathbf{n}_x$ is a unit vector along the x axis. As a representative value of the period, we choose $2x_0 = 7\ \mu$m; this gives $G \simeq 0.9 \times 10^4$ cm^{-1}. As the thickness of the domain walls is negligibly small, the periodicity of PPLN structure does not influence the linear optical properties of the medium. They are characterized by the ordinary (n_o) and extraordinary (n_e) refractive indices.

The photorefractive nonlinearity is caused by light-induced charge separation leading to spatial variations of the optical permittivity tensor $\delta\hat{\epsilon}$ owing to the linear electro-optic effect. It is important that the tensor of the
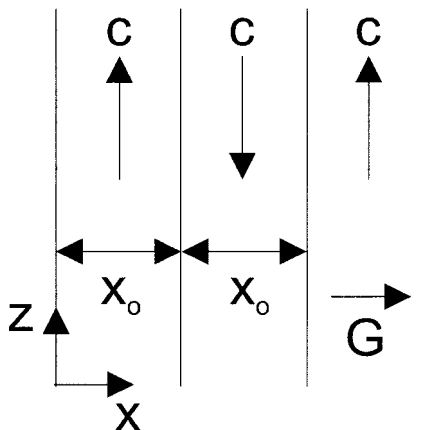

Fig. 1. Geometric diagram of the PPLN domain structure.

linear electro-optic effect is a polar characteristic; it is different in sign in positive and negative domains. Therefore we can write for the Cartesian components of the permittivity tensor

$$\delta\epsilon_{mn}(\mathbf{r}) \simeq -n^4 r_{mnl}E_l(\mathbf{r})p(x), \qquad (1)$$

where $n = (n_o + n_e)/2 \simeq n_{o,e}$ is the average refractive index, r_{mnl} is the conventional electro-optic tensor, E_l is the lth component of the electric field, and $p(x)$ is a periodic function equal to $+1$ and -1 in the positive and negative domains, respectively. The largest independent components of the electro-optic tensor r_{mnl} are $r_{333} \equiv r_{33}$, $r_{113} \equiv r_{13}$, and $r_{131} \equiv r_{51}$. The components r_{33} and r_{13} are responsible for coupling between waves of the same type of polarization, extraordinary (e) and ordinary (o), respectively, whereas the component r_{51} is responsible for coupling between o and e waves.

In our next step we define the relevant mechanisms of light-induced charge transport in PPLN. These mechanisms are the photovoltaic effect, drift, and diffusion of photoexcited electrons.[14,15] It is essential that the photovoltaic effect, in contrast to drift and diffusion, is polar in nature; the direction of the photovoltaic current is opposite in the plus and minus domains. Let **A** be the complex slowly varying (in time but not in space) amplitude of the light electric field vector so that $I = |\mathbf{A}|^2$ is the light intensity. Then the expression for the mth component of the current density **j** can be presented in the form

$$j_m = p(x)\beta_{mnl}A_nA_l^* + \kappa(E_m + k_BTe^{-1}\nabla_m)|\mathbf{A}|^2, \quad (2)$$

where β_{mnl} is the photovoltaic tensor, κ the specific photoconductivity, k_B is the Boltzman constant, T is the absolute temperature, and e is the elementary charge. Only the first term is here an alternating function of x. The second and third terms, characterizing the drift and diffusion contributions, are free of the influence of the periodic structure. We have neglected in Eq. (2) the anisotropy of the photoconductivity, which is well justified for LiNbO$_3$ crystals.

The photovoltaic tensor is generally complex; it can be presented in the form[14]

$$\beta_{mnl} = \beta_{mnl}^L + i\,\delta_{mnk}\beta_{kl}^C, \qquad (3)$$

where $\hat{\beta}^L$ and $\hat{\beta}^C$ are the real tensors describing the so-called linear and circular photovoltaic currents and δ_{mnk} is the antisymmetric unit tensor. The tensor β_{mnl}^L is symmetric to permutation of n and l. Its independent components are $\beta_{33}^L \equiv \beta_{333}^L$, $\beta_{31}^L \equiv \beta_{311}^L$, and $\beta_{15}^L \equiv \beta_{131}^L$. The components β_{33}^L and β_{31}^L correspond to the currents induced in the z direction by light polarized along and perpendicular to the optical axis, respectively. The component β_{15}^L corresponds to a current directed perpendicular to the polar axis; to excite this current, the light field should possess simultaneously the components parallel and perpendicular to the optical axis. In other words, o and e waves should be present simultaneously in the crystal. The component β_{12}^C is also responsible for the transverse photovoltaic current induced by o and e waves. Since the wave vectors of these waves are different, the transverse currents are always spatially oscillating. The main difference between the transverse spatially oscillat-

ing currents related to β_{15}^L and β_{12}^C is that they are shifted to each other by a quarter of a period. This difference is important for nonlinear optical effects.

The ratios β_{mnl}/κ characterize the light-induced photovoltaic fields. In LiNbO$_3$ doped with Fe or Cu the longitudinal fields E_{33}^L and E_{31}^L range from a few tens to 100 kV/cm. The transverse fields E_{15}^L and E_{12}^C are roughly smaller by one order of magnitude. The effects related to the longitudinal and transverse photovoltaic currents are distinguished by different polarization and orientation properties.[13,14] Usually the photovoltaic transport is dominating in photorefractive LiNbO$_3$.

Note that the above phenomenological expression (2) for the light-induced current is valid when the characteristic scale of spatial changes of **A** is greater than the characteristic transport lengths of the material; see Ref. 16 for more details. In LiNbO$_3$ this condition is usually fulfilled up to the scale comparable with light wave length.

3. PHASE-MATCHING CONDITIONS AND QUALITATIVE CONSIDERATION OF SCATTERING PROCESSES

Parametric scattering processes are typically specified by proper phase-matching conditions for light wave vectors. These conditions carry also a great deal of information about the general features of the parametric processes. The relevant description for the single-domain case can be found in Ref. 13. The presence of the periodic PPLN structure results (i) in modification of the characteristics of the processes known in single-domain LiNbO$_3$ crystals and (ii) in qualitatively new scattering processes. The fingerprint of a new parametric process is the presence of the vector of the periodic structure **G** in the corresponding phase-matching condition. Below we consider several representative examples of parametric four-wave processes in PPLN.

A. Processes Known for the Single-Domain Case

We consider first two processes, A: $ee \rightarrow ee$ and B: $ee \rightarrow ee$, in which two extraordinary (e) pump waves $p1, p2$ transform into scatter e waves $s1, s2$. The relevant phase-matching conditions are

$$\mathbf{k}_{p1}^e + \mathbf{k}_{p2}^e = \mathbf{k}_{s1}^e + \mathbf{k}_{s2}^e, \tag{4a}$$

$$\mathbf{k}_{p1}^e - \mathbf{k}_{p2}^e = \mathbf{k}_{s1}^e - \mathbf{k}_{s2}^e. \tag{4b}$$

They are illustrated by Figs. 2(a) and 2(b). One sees that for the A process, and pair of diametrically opposed wave vectors $\mathbf{k}_{s1}^e$, $\mathbf{k}_{s2}^e$ meets Eq. (4a), i.e., the scatter waves form on a screen (placed in the far field) a light ring passing the pump spots. For the B process the scatter waves $s1, s2$ form two vertical lines passing the pump spots.

Experimental manifestations of the above processes in the single-domain and PPLN parts of our 3-mm-thick sample (see Ref. 12 for more details) are presented in Figs. 3(a) and 3(b), respectively. The rings and vertical lines correspond to A and B processes. Qualitatively, the light distributions in the subfigures (a) and (b) are similar.
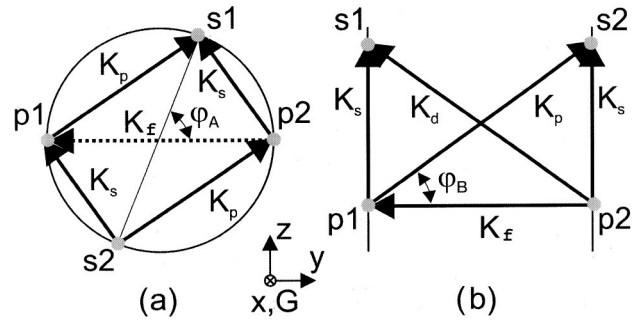

Fig. 2. Schematic diagram of the wave and grating vectors for the processes (a) A: $ee \rightarrow ee$ and (b) B: $ee \rightarrow ee$. The gray dots mark the tips of the wave vectors.
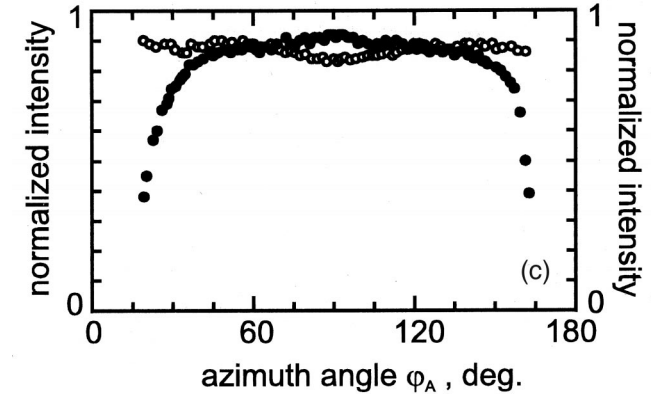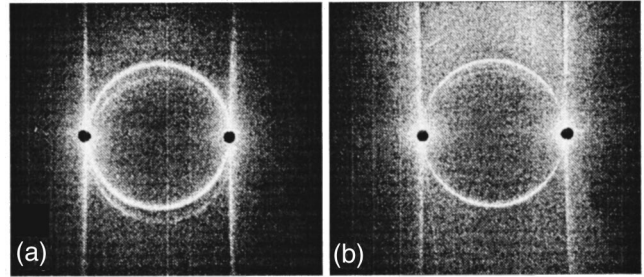

Fig. 3. Far-field distributions of scattered light for (a) the single-domain and (b) PPLN parts of the sample. Image doubling is due to reflection from the output face. (c) Azimuth dependence of the ring intensity; the open and filled dots correspond to the cases (a) and (b), respectively.

The diagrams presented in Fig. 2 allow comment on the mechanism of spatial amplification of scattered waves. This mechanism is different for the A and B processes.

In the case A, two refractive-index gratings, s and p, are involved in amplification of the waves $s1, s2$. Two wave pairs, $s1, p2$ and $p1, s2$, contribute to recording of the s grating (the grating vector $\mathbf{K}_s = \mathbf{k}_{s1}^e - \mathbf{k}_{p2}^e \equiv \mathbf{k}_{p1}^e - \mathbf{k}_{s2}^e$). The other two pairs, $s1, p1$ and $p2, s2$, contribute to the p grating (the grating vector $\mathbf{K}_p = \mathbf{k}_{s1}^e - \mathbf{k}_{p1}^e \equiv \mathbf{k}_{p2}^e - \mathbf{k}_{s2}^e$). Diffraction of the pump waves $p1$ and $p2$ from the gratings p and s, respectively, increases the wave $s1$. Similarly, diffraction of the waves $p1$ and $p2$ from the gratings s and p, respectively, amplifies the wave $s2$. Mutually coupled recording and diffraction processes result in spatial amplification of weak seed waves at the expense of the pump.[13] The rate of spatial amplification (brightness of the scatter ring) depends on

the azimuth angle φ_A. This is clearly seen from the experimental Fig. 3(c).

In the case B, four gratings, s, p, d, and f, are responsible for the spatial amplification. Only the s grating [see Fig. 2(b)] is contributed here by two wave pairs, $s1$, $p1$ and $s2$, $p2$. The f grating is formed by the pump waves, and it allows for mutual diffraction of weak waves $s1$ and $s2$. Brightness of the lines depends on the distance from the pump spots; see Fig. 3(a).

The distinctive features of the above parametric processes in PPLN can be explained qualitatively as follows. Because of the periodic PPLN structure, the electro-optic coefficient r_{33}, responsible for diffraction of e waves, changes periodically its sign along the x coordinate; see Fig. 1. Therefore in contrast to the single-domain case the amplitude of a refractive-index grating cannot be obtained by multiplying of the corresponding amplitude of the space-charge field by r_{33}. Instead, it is necessary to find the dependence $E_{\mathrm{sc},z}(\mathbf{r})$, to multiply it by $r_{33}(\mathbf{r})$, and then to calculate the necessary Fourier component. Performed in Ref. 9, this procedure shows a considerable decrease of the photorefractive response at the spatial frequency $K \ll G$. As applied to the above scattering patterns in PPLN, this should result in decreasing brightness of the light ring and lines in the vicinity of the pump spots. This feature is clearly seen in Fig. 3(c).

The above-considered A and B processes belong to the simplest and strongest in LiNbO$_3$ crystals with dominating photovoltaic transport. At the same time, many other strong parametric processes are known in this material.[13] They manifest themselves in a variety of light rings and lines different in position and polarization. Most of the parametric processes can be observed simultaneously in the single-domain and PPLN cases.

B. New Scattering Processes

Phase-matching conditions for new scattering processes include not only light wave vectors but also the vector of the periodic structure $\mathbf{G}$. The new processes can be separated into two groups. The processes of the first group can run only for certain special values of the half-angle θ_p between the pump beams; they manifest themselves as dots (spots) of scatter light.

As the first example, we consider the process $2G$: $ee \rightarrow ee$ defined by the phase-matching condition

$$\mathbf{k}_{2s}^e - \mathbf{k}_{2p}^e + 2\mathbf{G} = \mathbf{k}_{1p}^e - \mathbf{k}_{1s}^e - 2\mathbf{G} = \mathbf{K}, \qquad (5)$$

where $\mathbf{K} = \mathbf{k}_{2p}^e - \mathbf{k}_{1p}^e$ and the pump beams propagate symmetrically to the x axis in the x,z plane. The corresponding wave-vector diagram is shown in Fig. 4(a). The phase-matching condition specifies both the pump angle θ_p and the scatter angle θ_s.

A qualitative explanation of appearance of the scatter waves $s1$ and $s2$ is as follows. The pump waves $p1$ and $p2$ record a refractive-index grating. In PPLN, this grating possesses not only the main spatial frequency $\mathbf{K}$ but also the side harmonics $\mathbf{K} \pm \mathbf{G}$, $\mathbf{K} \pm 2\mathbf{G}$, etc. Diffraction of the pump waves from the side grating $\mathbf{K} \pm 2\mathbf{G}$ gives just the waves $1s$ and $2s$.

Instead of $2\mathbf{G}$, we can set in Eq. (5) the vector $\mathbf{G}$. Correspondingly, instead of the above $2G$ process we obtain a $1G$ process with new expected values of θ_p and θ_s. In
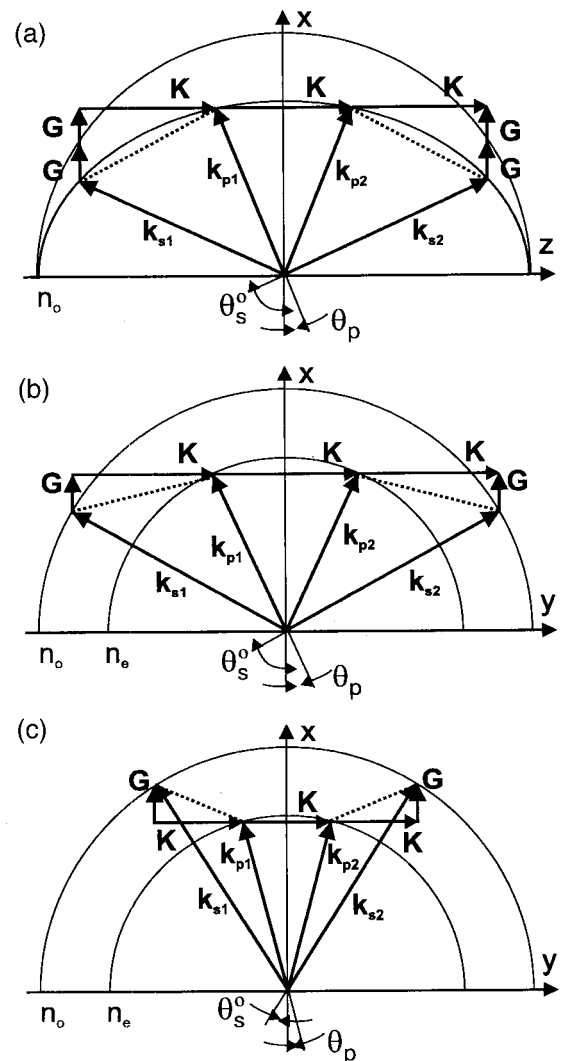

Fig. 4. Wave-vector diagrams for the processes responsible for the generation of anomalous light dots in PPLN; the cases (a) and (b), (c) correspond to $1G$: $ee \rightarrow ee$ and $1G$: $ee \rightarrow oo$ processes, respectively.

reality, this $1G$ process is much weaker in PPLN as compared with the $2G$ process. The reason for this lies beyond our qualitative considerations; it is explained in Section 5.

Figures 5(a) and 5(b) show two scattering patterns obtained in the PPLN and single-domain parts of our sample under the same experimental conditions. The side spots in Fig. 5(a) (of the extraordinary polarization) correspond to the $s1$ and $s2$ scattered waves. No side spots can be seen in Fig. 5(b). The experimental values of the angles θ_p and θ_s are in a good agreement with those calculated for the $2G$ process.

Another process of the first group is $1G$: $ee \rightarrow oo$; it gives scatter waves different in polarization from the pump. The corresponding phase-matching condition is

$$\mathbf{k}_{s1}^o - \mathbf{k}_{p1}^e \pm \mathbf{G} = \mathbf{k}_{p2}^e - \mathbf{k}_{s2}^o \mp \mathbf{G} = -\mathbf{K}^{\pm}. \qquad (6)$$

Two e-polarized pump beams propagate in the xy plane symmetrical to the x axis. The upper and lower signs in Eq. (6) correspond to two different diagrams shown in Figs. 4(b) and 4(c). For the upper signs [Fig. 4(b)] the

pump and scatter angles can be estimated for our sample as $\theta_p^+ \simeq 17.6°$ and $\theta_s^+ \simeq 65.3°$, whereas for the lower signs [Fig. 4(c)] we have $\theta_p^- \simeq 6.6°$ and $\theta_s^- \simeq 20.4°$.

The corresponding experimental data for PPLN are shown in Figs. 6(a) and 6(b). The polarizations of the pump and scatter waves are mutually orthogonal. They, as well as the actual angles, meet the above phase-matching conditions with a high accuracy.

Qualitative explanation of the anomalous *o* spots is similar to that given above for the *e* dots. The pump beams record a grating of the optical permittivity $\delta\epsilon_{13}(\mathbf{r})$, which includes not only the fundamental frequency $\mathbf{K}$ but also the side harmonics $\mathbf{K} \pm \mathbf{G}$. The *e*-polarized pump beams diffract from these side gratings into *o* waves exploiting the electro-optic coefficient $r_{51} \approx 28$ pm/V, which is comparable with the biggest (for LiNbO$_3$) coefficient $r_{33} \approx 30$ pm/V. It is interesting that the strong process under study involves $1G$ side gratings. Recording of $2G$ side harmonics (compare with the previous case) is not necessary here. An explanation of this difference is given in Section 6.

Let us touch lastly on the anomalous parametric processes of the second group. The phase-matching conditions for them can be obtained from the conditions known for single-domain crystals [like Eqs. (4)] by adding in the
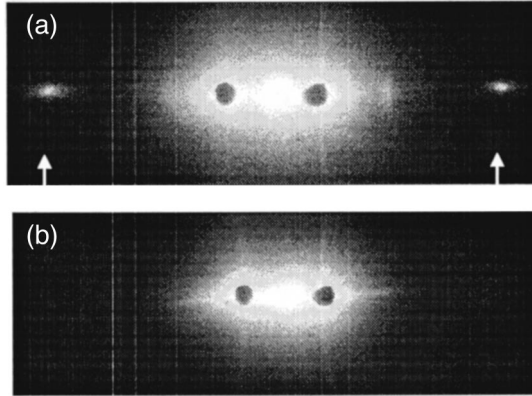

Fig. 5. Far-field intensity distributions for $2G$: $ee \rightarrow ee$ scattering process; the patterns (a) and (b) are obtained in PPLN and single-domain parts of the sample, respectively. The central pump spots are shadowed by small disks.
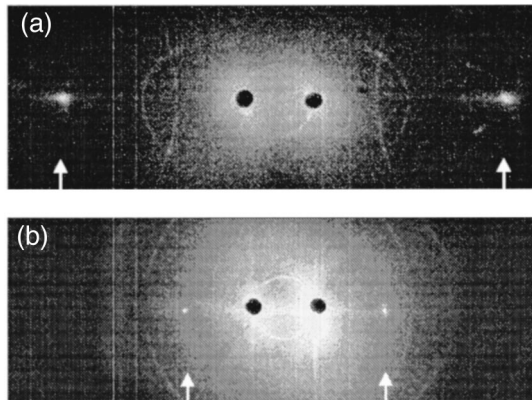

Fig. 6. Far-field intensity distribution for $1G$: $ee \rightarrow oo$ scattering process; the central (pump) and side (scatter) light beams are *e* and *o* polarized, respectively.

right-hand side the vectors $\mathbf{G}$, $2\mathbf{G}$, etc. The corresponding processes run without any fine adjustment of the pump angle, and they result in additional scatter rings and lines. The relevant light patterns have been detected experimentally (see, e.g., Fig. 6), but they are typically weaker in our sample as compared with the "normal" light rings and lines.

4. PHOTOREFRACTIVE RESPONSE OF PPLN

Let the light field be superposition of two waves with wave vectors $\mathbf{k}_1$ and $\mathbf{k}_2$ so that

$$\mathbf{A} = \mathbf{A}_1 \exp(i\mathbf{k}_1 \cdot \mathbf{r}) + \mathbf{A}_2 \exp(i\mathbf{k}_2 \cdot \mathbf{r}). \tag{7}$$

In a single-domain crystal this would result in generation of the fundamental grating of a space-charge field with the grating vector $\mathbf{K} = \mathbf{k}_1 - \mathbf{k}_2$ and also higher harmonics with spatial frequencies $2\mathbf{K}$, $3\mathbf{K} \ldots$. Smallness of the higher harmonics is ensured by smallness of the ratio $|\mathbf{A}_1 \cdot \mathbf{A}_2^*|/I_0$, where $I_0 = |\mathbf{A}_1|^2 + |\mathbf{A}_2|^2$ is the total light intensity. For most of photorefractive effects the higher harmonics are of minor importance.

The periodic PPLN structure results in a strong modification of the spectrum of spatial frequencies presented in the light-induced variation of the optical permittivity. Instead of the fundamental spatial frequency $\mathbf{K}$, a sequence of spatial harmonics, $\mathbf{K} + s\mathbf{G}$, where $s = 0, \pm1, \pm2 \ldots$, is expected to be excited. Moreover, the side harmonics with $s = \pm1, \pm2, \ldots$ should not be small in the general case because of an ultimately strong periodic spatial modulation of the transport and electro-optic properties expressed by the alternating function $p(x) = \pm1$.

To characterize the photorefractive response of PPLN, we have to first calculate the space-charge field $\mathbf{E}_{sc}(\mathbf{r})$ and then find the spatial harmonics $\mathbf{E}_K^{(s)}$ presented in the Fourier expansion

$$p\mathbf{E}_{sc} = \sum_s \mathbf{E}_K^{(s)} \exp[i(\mathbf{K} + s\mathbf{G}) \cdot \mathbf{r}] + \text{c.c.} \tag{8}$$

Then, in accordance with Eq. (1), description of the light-induced change of the permittivity tensor $\delta\hat{\epsilon}(\mathbf{r})$ reduces to a simple algebraic problem.

With the higher harmonics $2K$, $3K,\ldots$ neglected, the contributions to $\delta\hat{\epsilon}(\mathbf{r})$ caused by drift plus diffusion and photovoltaic effect become independent. It is convenient to consider them separately.

Since the first two transport mechanisms are insensitive to the presence of the periodic structure [see Eq. (2)], their contributions to $\mathbf{E}_{sc}$ are the same as in the single-domain case, and calculation of $\mathbf{E}_K^{(s)}$ reduces to calculation of Fourier harmonics of $p(x)$. Correspondingly, we have for the drift–diffusion contribution

$$\mathbf{E}_K^{(s)} = \frac{2i\mathbf{n}}{s\,\pi}(\mathbf{n} \cdot \mathbf{E}_0 + iE_D)\frac{\mathbf{A}_1 \cdot \mathbf{A}_2^*}{I_0}, \tag{9}$$

where $\mathbf{E}_0$ is an externally applied electric field, $E_D = k_B T/e$ is the diffusion field, $\mathbf{n} = \mathbf{K}/K$ is the unit fundamental grating vector, and the number s takes only the odd values $\pm1, \pm3,\ldots$ All the harmonics with even s, in-

cluding $\mathbf{E}_K^{(0)}$, turn to zero. This result is not different from that found in Ref. 9. This means, in particular, that two light waves cannot be coupled in PPLN through the fundamental grating in the case of drift–diffusion transport. As follows from Eq. (9), the nonzero harmonics $\mathbf{E}_K^{(s)} \propto \mathbf{n}$ and their amplitudes decrease rather slowly with increasing s. Note that the value $m = 2|\mathbf{A}_1 \cdot \mathbf{A}_2^*|/I_0$ is the contrast of the light interference pattern.

Characterization of the photovoltaic contribution, which is usually dominating in LiNbO$_3$, is a more difficult problem. The point is that the photovoltaic transport is sensitive to the periodic alternation of the polar axis [see Eq. (2)]. For this reason, the problem of calculation of $\mathbf{E}_{sc}(\mathbf{r})$ is not one dimensional. Under some simplifying assumptions, which were too strong for the purposes of our study, this problem was solved in Ref. 9. Referring the reader to Appendix A for details, we present here the final result,

$$\mathbf{E}_K^{(s)} = -\frac{K_\perp}{K^2 x_0}\left[\frac{q(\boldsymbol{\nu}\cdot\boldsymbol{\mathcal{E}})\boldsymbol{\nu}}{q^* - isG}\tanh\left(\frac{q^* x_0}{2}\right)\right.$$

$$\left. + \frac{q^*(\boldsymbol{\nu}^*\cdot\boldsymbol{\mathcal{E}})\boldsymbol{\nu}^*}{q + isG}\tanh\left(\frac{q x_0}{2}\right)\right] - \mathbf{n}(\boldsymbol{\mathcal{E}}\cdot\mathbf{n})\delta_{s0},$$

(10)

where δ_{s0} is the Kronecker symbol, $\boldsymbol{\nu} = \mathbf{n}_x + i\mathbf{n}_\perp$, $q = K_\perp + iK_x$, the subscript $\perp$ refers to the component perpendicular to $\mathbf{n}_x$, and mth component of the effective (generally complex) photovoltaic field $\boldsymbol{\mathcal{E}}$ is defined by $\mathcal{E}_m = \beta_{mnl}A_n A_l^*/\kappa I_0$. Note that Eq. (10) is valid only for even numbers, $s = 0, \pm 2,\ldots$. For odd numbers, $\mathbf{E}_K^{(s)} = 0$. This circumstance comes from the polar nature of the photovoltaic transport.

The main difference between Eq. (10) and a similar equation derived in Ref. 9 is in an arbitrary orientation of the vector $\boldsymbol{\mathcal{E}}$. In particular, this vector can have a nonzero x component, which means that the photovoltaic current is not parallel to the domain walls. This means, in turn, charging of the domain walls.

Particular Cases

A. $\boldsymbol{\mathcal{E}},\mathbf{K}\|\mathbf{n}_z$. A geometrical diagram for this case is shown in Fig. 7(a). Waves 1 and 2 are of the same type here (e or o), the interference fringes are perpendicular to the domain walls and the photovoltaic current, characterized by either β_{33}^L or β_{31}^L, is perpendicular to the fringes and parallel to the domain walls. In this case we have $K_x = 0$, $K_\perp = K$, and $q = K$. Furthermore, instead of the vectorial wave amplitudes $\mathbf{A}_{1,2}$, we can use here the scalar amplitudes $A_{1,2}$. Then Eq. (10) gives for the first two nonzero spatial harmonics

$$\mathbf{E}_K^{(0)} = -\mathbf{n}_z E_{pv}\left[1 - \frac{2}{Kx_0}\tanh\left(\frac{Kx_0}{2}\right)\right]\frac{A_1 A_2^*}{I_0},$$

$$\mathbf{E}_K^{(2)} = E_{pv}\tanh\left(\frac{Kx_0}{2}\right)\frac{(Kx_0/2)\mathbf{n}_z + \pi\mathbf{n}_x}{(Kx_0/2)^2 + \pi^2}\frac{A_1 A_2^*}{I_0},$$

(11)

where E_{pv} is E_{33}^L and E_{31}^L for e and o waves, respectively. The result for the fundamental amplitude $\mathbf{E}_K^{(0)}$ coincides
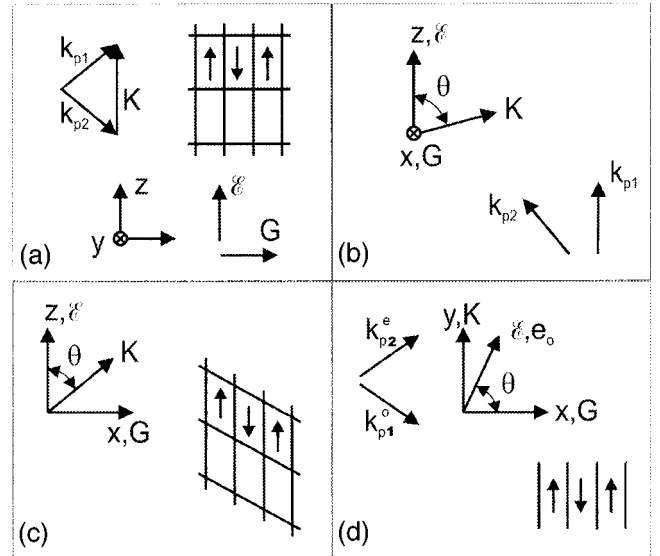

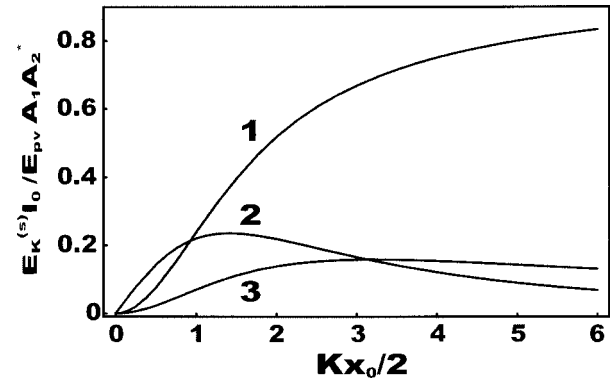Fig. 7. Geometric diagrams for four different cases of grating recording in PPLN.

Fig. 8. Dependence of the harmonics $E_K^{(0)}$, $E_{K,z}^{(2)}$, and $E_{K,x}^{(2)}$ on $Q = Kx_0/2$ (curves 1, 2, and 3, respectively) for the photovoltaic transport in the case (a) of Fig. 7.

with that obtained in Ref. 9. We see that the fundamental harmonic has only a z component. For $Kx_0/2 \gg 1$ its value corresponds to the single-domain case. As seen from Eq. (11), the periodic structure does not change the π shift between the fundamental spatial harmonic and the light interference pattern. The first nonzero side harmonic, $\mathbf{E}_K^{(2)}$, has not only a z but also an x component. The dependences of $E_K^{(0)}$, $E_{K,z}^{(2)}$, and $E_{K,x}^{(2)}$ on the product $Q = Kx_0/2$ are shown in Fig. 8. Whereas $E_K^{(0)}(Q)$ grows monotonically from zero to its saturated value equal one, the functions $E_{K,z}^{(2)}(Q)$ and $E_{K,x}^{(2)}(Q)$ experience maxima at $Q \approx 1.4$ and 3 and then tend to zero. The maximum values of $E_{K,z}^{(2)}$ and $E_{K,x}^{(2)}$ are noticeably smaller than one.

In accordance with Eq. (1), the fundamental harmonic $\mathbf{E}_K^{(0)}$ modulates the diagonal elements of the permittivity tensor (i.e., the extraordinary and ordinary refractive indices) at the spatial frequency $\mathbf{K}$, but it does not produce any changes in the nondiagonal elements of $\hat{\epsilon}$. The light-induced changes $\delta\epsilon_{33}$ and $\delta\epsilon_{11}$ are proportional to the electro-optic constants r_{33} and r_{13}; they allow for mutual diffraction of e and o waves, respectively. The first side harmonic $\mathbf{E}_K^{(2)}$ produces the changes of both diagonal and

nondiagonal elements of the permittivity tensor. The latter are proportional to the electro-optic constant r_{51} and allow for anisotropic ($o - e$) diffraction of auxiliary (Bragg matched to the spatial frequency $\mathbf{K} + 2\mathbf{G}$) ordinary or extraordinary light beams.

B. $\boldsymbol{\mathcal{E}} \| \mathbf{n}_z$, $\mathbf{K} \perp n_x$, $\mathbf{K} \| \mathbf{n}_z$.   The corresponding diagram is shown in Fig. 7(b).   Here θ is the angle between $\mathbf{K}$ and $\boldsymbol{\mathcal{E}}$. The expressions for $\mathbf{E}_K^{(0)}$ and $\mathbf{E}_K^{(2)}$ can be obtained from Eqs. (11) by the replacement $E_{pv} \rightarrow E_{pv} \cos \theta$, $\mathbf{n}_z \rightarrow \mathbf{n}$. The changes of the refractive indices are smaller here by a factor of $\cos^2 \theta$ as compared with the case A.

C. $\boldsymbol{\mathcal{E}} \| \mathbf{n}_z$, $\mathbf{K} \in x$, z plane.   The relevant geometrical scheme is shown in Fig. 7(c).   The angle between $\mathbf{n}_z$ and $\mathbf{K}$ we again denote θ so that $K_x = K \sin \theta$, $K_\perp = K \cos \theta$, $q = K \exp(i\theta)$, and $\boldsymbol{\nu} = \mathbf{n}_x + i\mathbf{n}_z$.   Using Eq. (10), we obtain for the fundamental amplitude

$$E_{K,z}^{(0)} = E^{pv} \cos \theta (Q^{-1} \mathrm{Re}\{\exp(2i\theta)$$
$$\times \tanh[Q \exp(-i\theta)]\} - \cos \theta) A_1 A_2^* / I_0,$$

$$E_{K,x}^{(0)} = E^{pv} \cos \theta (Q^{-1} \mathrm{Im}\{\exp(2i\theta)$$
$$\times \tanh[Q \exp(-i\theta)]\} - \sin \theta) A_1 A_2^* / I_0.$$
$$(12)$$

The z component is responsible for the effects of coupling between e or o waves (isotropic diffraction). Figure 9 shows the function $E_{K,z}^{(0)}(\theta)$ for three representative values of $Q = Kx_0/2$. This function is decreasing from the initial value that corresponds to the case A ($\mathbf{K} \| \mathbf{G}$) to zero value at $\theta = \pi/2$ ($\mathbf{K} \perp \mathbf{G}$). A highly pronounced plateau for $Q = 1.5$ (curve 2) looks surprising at first sight. This peculiarity is caused by proximity of the spatial resonance $\mathbf{K} = \mathbf{G}$ at $\theta = \pi/2$. One can find out that the limiting value of the ratio shown in Fig. 9 is $4/\pi^2 \cong 0.405$ for $Q \rightarrow \pi/2$ and $\theta \rightarrow \pi/2$; this is only slightly smaller than the initial value of $\simeq 0.416$ of the same ratio at $Q = \pi/2$.

D. $\mathbf{K} \| \mathbf{n}_y$, $\boldsymbol{\mathcal{E}} \perp \mathbf{n}_z$.   This is the case when the transverse photovoltaic current is responsible for grating recording, and this current is not parallel to the domain walls [see Fig. 7(d)]. Here we have $K_x = 0$, $K_\perp = K$, $q = K$, and
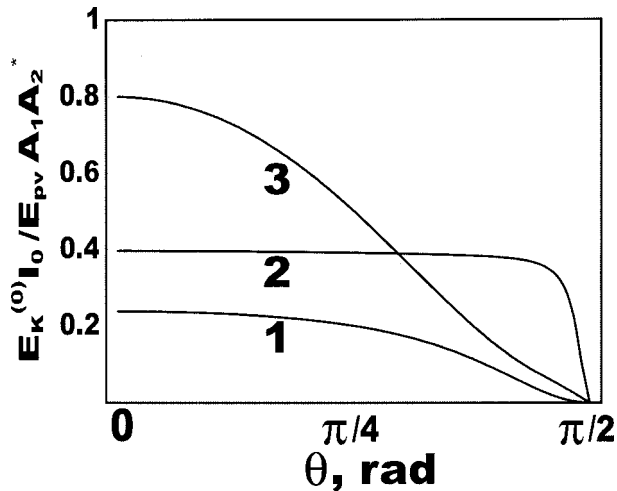

Fig. 9.   Dependence $E_K^{(0)}(\theta)$ for different values of $Q = Kx_0/2$ in the case (c) of Fig. 7.   Curves 1, 2, and 3 are plotted for $Q = 1$, 1.5, and 5, respectively.

$\boldsymbol{\nu} = \mathbf{n}_x + i\mathbf{n}_y$.   The waves 1 and 2 are assumed to be ordinary and extraordinary, respectively; they do not produce any spatial modulation of light intensity. To specify the vector $\boldsymbol{\mathcal{E}}$, it is useful to represent the vectorial wave amplitudes in the form $\mathbf{A}_{1,2} = \mathbf{e}_{o,e} A_{o,e}$, where $\mathbf{e}_{o,e}$ are the unit polarization vectors and $A_{o,e}$ are the scalar amplitudes. Then, using the results of Section 2, we have $\boldsymbol{\mathcal{E}} = \mathbf{e}_o (E_{15}^L - iE_{12}^C) A_0 A_e^* / I_0$. The angle between the vector $\mathbf{e}_o$ and the x axis we denote θ. Using Eq. (10), we obtain then for the fundamental component of the space-charge field

$$\mathbf{E}_K^{(0)} = (E_{15}^L - iE_{12}^C)[\mathbf{n}_x \cos \theta Q^{-1} \tanh Q$$
$$+ \mathbf{n}_y \sin \theta (1 - Q^{-1} \tanh Q)] A_o A_e^* / I_0.   (13)$$

It is interesting that the x component of $\mathbf{E}_K^{(0)}$ tends to zero for $Kx_0 \rightarrow \infty$, whereas the y component tends to a nonzero limiting value, and this value does not correspond to the single domain case. This feature is general for the situations where $\boldsymbol{\mathcal{E}} \| \mathbf{K}$.

The light-induced transverse field produces the change of the nondiagonal ($\delta\epsilon_{13}$) element of the permittivity tensor, and this change is proportional to the electro-optic coefficient r_{51}. This leads to coupling of orthogonally polarized o and e waves.

It is important to notice that in the above analysis we did not explicitly use the fact that the polar $\mathbf{c}$ axis (see Fig. 1) is perpendicular to the domain walls. At first sight, Eq. (10) is valid for an arbitrary orientation of the vectors $\mathbf{K}$, $\mathbf{G}$, and $\boldsymbol{\mathcal{E}}$ irrespective of orientation of $\mathbf{c}$. The problem is that in the case $\mathbf{c} \cdot \mathbf{G} \neq 0$ the longitudinal photovoltaic current results in generation of a strong periodically alternating electric field even in the absence of light-field modulation, $\mathbf{A}(\mathbf{r}) = \mathrm{const}$. This field modifies strongly the linear optical properties of the sample and leads perhaps to new optical effects.

5.   APPLICATIONS TO PARTICULAR SCATTERING PROCESSES

The technique for description of various parametric processes in the single-domain case is described in Ref. 13. In its main features, this technique is applicable to the above processes in PPLN. The main difference is in the appearance of proper correction factors in the expressions for the grating amplitudes and also in appearance of new spatial frequencies in the response of the medium to an exposing periodic light pattern. We illustrate below how this technique, in combination with the above results for the photorefractive response, can be applied to particular scattering processes observed in PPLN.

A.   Light Rings and Lines in PPLN Owing to $ee \rightarrow ee$ Processes

In this case (see also Figs. 2 and 3) the photovoltaic field E_{33}^L defines the charge separation, and the electro-optic constant r_{33} defines the rate of light diffraction. The relevant $\mathbf{K}$ vectors are perpendicular to $\mathbf{G}$, and they are not parallel to the z axis. This situation corresponds to case B of the previous section. If K is the length of the grating vector, the relevant correction factor for the grating amplitude is $F(Q) = 1 - \tanh(Q)/Q$, where $Q = Kx_0/2$. As

for the effect of tilt between **K** and the $\mathbf{n}_z$, it is the same for the single-domain and PPLN cases.

Now we can turn to calculations of the main characteristic of the parametric amplification, the rate of spatial exponential growth Γ, also often called the increment. We consider separately the characteristic features of Γ for the ring and the lines.

1. Angular Dependence of the Increment for the Ring
Using the results of Section 7 of Ref. 13 and parametrizing the position of the point $1s$ in Fig. 2(a) by the polar angle φ_A, which varies from 0 to 180°, we come to the following expression for the increment:

$$\Gamma_A = |\pi m_p n^3 r_{33} E_{33}^L/2\lambda| F_A(\varphi_A),$$

$$F_A = \cos^2(\varphi_A/2) F[Q \sin(\varphi_A/2)]$$

$$+ \sin^2(\varphi_A/2) F[Q \cos(\varphi_A/2)]. \quad (14)$$

Here $m_p = 2\sqrt{I_{p1}I_{p2}}/I_0$ is the contrast of the pump interference pattern, $Q = Kx_0/2$, and $K = 4\pi \sin \theta_p/\lambda$ is the pump grating vector. Two correction F factors entering the expression for F_A correspond to the s and p gratings in Fig. 2(a). To return to the single-domain case, one should set $F = 1$; we have then $F_A = 1$. At $m_p = 1$ and $\lambda = 514$ nm we have the numerical estimate Γ_A [cm^{-1}] $\approx F_A E_{33}^L$ [kV/cm]. Since E_{33}^L is often as high as several tens of kV/cm, the amplification factor for seed intensity, $\exp(2\Gamma_A d)$ ($d \simeq 3$ mm is the thickness of the sample), can be huge.

Figure 10(a) shows the angular dependence of F_A for three different values of the pump angle θ_p. One sees that near the pump spots, i.e., for $\varphi_A \simeq 0$, π, F_A is strongly decreasing. The curves are symmetric about the

point $\pi/2$ where Γ_A reaches its maximum. With increasing θ_p the factor F_A tends to 1. The described features are in a good qualitative agreement with experiment [see Fig. 3(c)].

2. Light Distribution Along the Lines
In this case, like in Ref. 13, we restrict ourselves to the case of equal intensities of the pump beams. To parametrize the positions of the points $s1$ and $s2$, we introduce the inclination angle φ_B, as shown in Fig. 2(b). As seen from this diagram, the longitudinal photovoltaic current can participate only in recording of the s, p, and d gratings. It is clear also that recording of and diffraction from the p and d gratings suffer from inclinations of the vectors $\mathbf{K}_p$ and $\mathbf{K}_d$ to the z axis. As for the s grating, which is contributed to by the wave pairs, $p1$, $s1$ and $p2$, $s2$, the relevant recording and diffraction processes possess no additional smallness. The above-described features result in the following modification of Eq. (42) of Ref. 13 for the increment:

$$\Gamma_B = |\pi n^3 r_{33} E_{33}^L/4\lambda| F_B,$$

$$F_B = 2F(Q \tan \varphi_B)$$

$$+ \sin^2 \varphi_B F(Q/\cos \varphi_B). \quad (15)$$

The value of Q is the same as in Eq. (14). The first and second contributions to the factor F_B correspond to the s and p, d gratings, respectively [see Fig. 2(b)]. For $F = 1$ we return to the result known for the single-domain case. Figure 10(b) shows the dependence $F_B(\varphi_B)$ for several values of θ_p. One sees that for small values of φ_B, i.e., in the vicinity of the pump spots, F_B (and Γ_B) is very small. This smallness is mostly due to a small correction factor for the s grating [see Fig. 2(b)]. The contributions from the p and d gratings are also small here because the corresponding grating vectors are almost perpendicular to the z axis. The larger θ_p is, the stronger is the dip near zero. With increasing φ_B the curves in Fig. 10(b) monotonously approach the value of 3. The described behavior of the increment near the pump spots corresponds qualitatively to the experimental data for the light-induced line presented in Fig. 3(b). The decrease of the line's intensity far from the pump spots is explained by a decreasing overlap between the pump and scattered beams.

B. Anomalous Light Dots
Here we apply the results of Section 4 to evaluate the efficiencies of the processes responsible for the appearance of anomalous light dots in PPLN. Qualitatively these processes were considered in Section 3.

1. Light Dots Owing to Isotropic Diffraction
Interpretation of the $2G$ process proposed in Section 3 requires calculation of the second side harmonic $E_{K,z}^{(2)}$. From Eq. (11) we obtain

$$\frac{E_{K,z}^{(2)}}{E_{33}^L} = \frac{m_p K x_0 \tanh(K x_0/2)}{K^2 x_0^2 + 4\pi^2}. \quad (16)$$

The product Kx_0 can be estimated from the corresponding phase-matching condition as ~ 24.7. This gives $|E_{K,z}^{(2)}|$
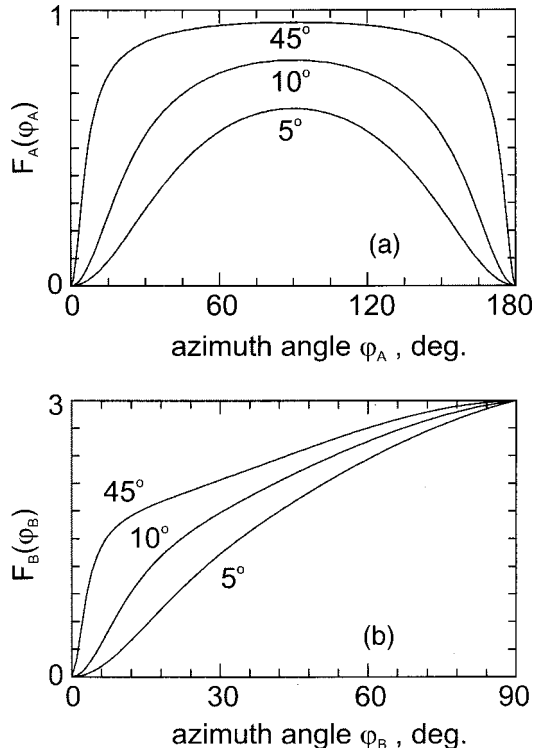

Fig. 10. Dependences (a) $F_A(\varphi_A)$ and (b) $F_B(\varphi_B)$ for three different values of the pump angle θ_p (in air) and $\lambda = 514$ nm.

$\simeq 0.04 E_{33}^L m_p$. Using further the standard equations of Bragg diffraction, we obtain for the sought intensities of the waves $s1$ and $s2$

$$(I_{1s}/I_{1p})^{1/2} = (I_{2s}/I_{2p})^{1/2} \approx \pi n^3 r_{33} d|E_{K,z}^{(2)}|/\lambda. \quad (17)$$

Using proper values of n, r_{33}, and the above estimate for $|E_{K,z}^{(2)}|$, we can estimate the square roots in Eq. (17) as $\sim 0.1 m_p d E_{33}^L$ with E_{33}^L measured in kV/cm. For $E_{33}^L < 30$ kV/cm, which is probably the actual case, the intensities $I_{1s,2s}$ are considerably smaller than the total pump intensity.

A similar phase-matched $2G$ process can be observed for o waves. The relevant estimates of the angles are not much different from those given above. As for the efficiency of this process, it can be estimated from Eq. (17) if we replace the electro-optic constant r_{33} by r_{13}.

Dispersion of the domain sizes can result in a decrease of the scattering efficiency because the phase matching can be fulfilled only in a part of the sample. Such a dispersion should also result in decreasing angular selectivity of the process.

Note that $1G$ processes (**G** instead of $2G$ in the phase-matching conditions) are forbidden within the photovoltaic model for the symmetric domain structure. Correspondingly, their efficiency has to include an additional small ratio E_D/E_{33}^L.

2. Light Dots Owing to Anisotropic Diffraction

In accordance with interpretation of these dots given in Section 3 [see also Figs. 4(b) and 4(c)], we have to calculate first the side harmonic $E_K^{(1)}$ induced by the pump beams. In the absence of an applied field, the only expected recording mechanism is diffusion of photoexcited electrons. As we know from Section 4, diffusion gives just odd-number side harmonics; the strongest of them is indeed $E_K^{(1)} \simeq m_p E_D/\pi$. The diffusion field $E_D = k_B T/e$ is expected to be much smaller in LiNbO$_3$:Fe than E_{33}^L and E_{31}^L. However, the diffusion-mediated side harmonic does not include the small correction factor typical of the photovoltaic recording for $Kx_0 \gg 1$. The rate of anisotropic ($e \to o$) diffraction of the pump beams from the side harmonic is characterized by the electro-optic constant $|r_{51}|$. Correspondingly, we have for intensities of the scattered o waves

$$(I_{1s}^o/I_{1p}^e)^{1/2} = (I_{2s}^o/I_{2p}^e)^{1/2} \approx m_p n^3 r_{51} E_D d/\lambda. \quad (18)$$

For the case shown in Fig. 4(b) we have $E_D \simeq 2$ kV/cm. This gives a fairly strong efficiency of the relevant process. For the case of Fig. 4(c) the diffusion field is approximately three times smaller, and the corresponding intensities are expected to be smaller by a factor of $\sim 10^{-1}$. Dispersion of the domain sizes decreases the observable dot's intensities.

6. CONCLUDING REMARKS

We have demonstrated that bulk periodically poled LiNbO$_3$ crystals admit a rich variety of parametric four-wave scattering processes. Some of them are known for single-domain crystals, but many nonlinear processes are essentially new. We have generalized the results on the photorefractive response of PPLN and have applied them to description of a number of particular scattering processes. This has allowed us to explain a number of distinctive features of scattering patterns observed in experiment.

We suppose that investigations of photorefractive PPLN are in an initial stage. Actually, only one bulk photorefractive PPLN sample has until now been available for experiment. Growth of deliberately doped PPLN crystals of different periods and orientation of spontaneous polarization is expected to extend considerably the range of available and controllable photorefractive properties.

APPENDIX A: CALCULATION OF SPACE-CHARGE FIELD FOR THE PHOTOVOLTAIC TRANSPORT

Since the problem of calculation of the space-charge field is a three-dimensional one, it is useful to express $\mathbf{E}_{sc}$ through the scalar electrostatic potential, $\mathbf{E}_{sc} = -\nabla \varphi$. Then we represent this potential as $\varphi(\mathbf{r}) = \varphi_K(x) \times \exp(i\mathbf{K} \cdot \mathbf{r}) +$ c.c., where $\varphi_K(x)$ is a $2x_0$-periodic function. Last, from the stationary continuity equation $\nabla \cdot \mathbf{j} = 0$ we obtain the differential equation for φ_K:

$$\left(\frac{d^2}{dx^2} + 2iK_x \frac{d}{dx} - K^2 \right) \varphi_K = ip(x)(\mathbf{K} \cdot \boldsymbol{\mathcal{E}}), \quad (A1)$$

where $\mathcal{E}_m = \beta_{mnl} A_n A_l^*/\kappa I_0$. In contrast to Ref. 9, we put no restrictions on orientation of the characteristic photovoltaic field $\boldsymbol{\mathcal{E}}$. In particular, this vector can have a nonzero x component, which means that the photovoltaic current is not parallel to the domain walls.

The second-order linear differential equation (A1) has to be solved within the negative, $[-x_0, 0]$, and positive, $[0, x_0]$, intervals. Its general solution has the form

$$\varphi_K^{\pm} = C_1^{\pm}\exp(q^*x) + C_2^{\pm}\exp(-qx) \mp i(\mathbf{K} \cdot \boldsymbol{\mathcal{E}})/K^2, \quad (A2)$$

where $q = K_{\perp} + iK_x$ and $K_{\perp}$ is the modulus of the projection of $\mathbf{K}$ to the plane perpendicular to $\mathbf{G}$ (see also Fig. 1). Four constants, $C_{1,2}^{\pm}$, have to be found from proper boundary conditions. Two of them, $\varphi_K^+(0) = \varphi_K^-(0)$ and $\varphi_K^+(x_0) = \varphi_K^-(-x_0)$, express continuity of φ_K at zero and periodicity. Two remaining conditions are obtained from the requirement of the continuity of the component j_x at the domain walls. They read

$$(d\varphi_K^+/dx)(0) - (d\varphi_K^-/dx)(0) = 2\mathcal{E}_x,$$

$$(d\varphi_K^+/dx)(x_0) - (d\varphi_K^-/dx)(-x_0) = 2\mathcal{E}_x. \quad (A3)$$

Using Eqs. (A2) and (A3) and the other two boundary conditions, we obtain, after some calculations,

$$C_1^{\pm} = \frac{q(\boldsymbol{\nu} \cdot \boldsymbol{\mathcal{E}})}{2K^2 \sinh(q^*x_0)} [1 - \exp(\mp q^*x_0)],$$

$$C_2^{\pm} = \frac{q^*(\boldsymbol{\nu}^* \cdot \boldsymbol{\mathcal{E}})}{2K^2 \sinh(qx_0)} [1 - \exp(\pm qx_0)], \qquad (A4)$$

where $\boldsymbol{\nu} = \mathbf{n}_x + i\mathbf{n}_\perp$ and $\mathbf{n}_\perp = \mathbf{K}_\perp/K_\perp$ is the unit vector perpendicular to the x axis and lying in the G, K plane.

The space-charge field is expressed through φ_K as

$$\mathbf{E}_{\text{sc}} = -(i\mathbf{K}\varphi_K + \mathbf{n}_x d\varphi_K/dx)\exp(i\mathbf{K} \cdot \mathbf{r}) + \text{c.c.} \quad (A5)$$

Multiplying $\mathbf{E}_{\text{sc}}(\mathbf{r})$ by $p(x)$ and calculating the coefficients of the Fourier expansion (8), we obtain Eq. (10).

REFERENCES

1. M. Yamada, N. Nada, M. Saitoh, and K. Watanabe, "First-order quasi-phase matched LiNbO$_3$ waveguide periodically poled by applying an external field for efficient blue second-harmonic generation," Appl. Phys. Lett. **62**, 435–437 (1993).
2. W. K. Burns, W. McElhanon, and L. Goldberg, "Second harmonic generation in field poled, quasi-phase-matched, bulk LiNbO$_3$," IEEE Photon. Technol. Lett. **6**, 252–254 (1994).
3. J. Webjörn, V. Pruneri, P. St. Russel, J. R. M. Barr, and D. C. Hanna, "Quasi-phase-matched blue light generation in bulk lithium niobate, electrically poled via periodic liquid electrodes," Electron. Lett. **30**, 894–895 (1994).
4. L. E. Myers, R. C. Eckhard, M. M. Fejer, R. L. Byer, W. R. Bosenberg, and J. R. Pierce, "Quasi-phase-matched optical parametric oscillators in bulk periodically poled LiNbO$_3$," J. Opt. Soc. Am. B **12**, 2102–2116 (1995).
5. N. G. R. Broderick, G. W. Ross, H. L. Offerhaus, D. G. Richardson, and D. C. Hanna, "Hexagonally poled lithium niobate: a two-dimensional nonlinear photonic crystal," Phys. Rev. Lett. **84**, 4345–4348 (2000).
6. M. Taya, M. C. Bashew, and M. M. Fejer, "Photorefractive effect in periodically poled ferroelectrics," Opt. Lett. **21**, 857–859 (1996).
7. V. Pruneri, P. G. Kazansky, J. Webjörn, P. St. Russel, and D. C. Hanna, "Self-organized light-induced scattering in periodically poled lithium niobate," Appl. Phys. Lett. **67**, 1957–1959 (1995).
8. B. I. Sturman, M. Aguilar, F. Agullo-Lopez, V. Pruneri, P. G. Kazansky, and D. C. Hanna, "Mechanism of self-organized light-induced scattering in periodically poled lithium niobate," Appl. Phys. Lett. **69**, 1349–1451 (1997).
9. B. Sturman, M. Aguilar, F. Agullo-Lopez, V. Pruneri, and P. G. Kazansky, "Photorefractive nonlinearity of periodically poled lithium niobate," J. Opt. Soc. Am. B **14**, 2641–1649 (1997).
10. E. V. Podivilov, B. I. Sturman, G. F. Calvo, F. Agullo-Lopez, M. Carrascosa, and V. Pruneri, "Effect of domain structure fluctuations on the photorefractive response of periodically poled lithium niobate," Phys. Rev. B **62**, 13182–13187 (2000).
11. S. Odoulov, T. Tarabrova, A. Shumelyuk, I. I. Naumova, and T. O. Chaplina, "Photorefractive response of bulk periodically poled LiNbO$_3$:Y:Fe at high and low spatial frequencies," Phys. Rev. Lett. **84**, 3294–3297 (2000).
12. M. Goul'kov, S. Odoulov, I. Naumova, F. Agullo-Lopez, G. Calvo, E. Podivilov, B. Sturman, and V. Pruneri, "Degenerate parametric light scattering in periodically poled LiNbO$_3$:Y:Fe," Phys. Rev. Lett. **86**, 4021–4024 (2001).
13. B. I. Sturman, S. G. Odoulov, and M. Yu. Goul'kov, "Parametric four-wave processes in photorefractive crystals," Phys. Rep. **275**, 199–254 (1996).
14. B. I. Sturman and V. M. Fridkin, *The Photovoltaic and Photorefractive Effects in Noncentrosymmetric Materials* (Gordon and Breach, Philadelphia, 1992).
15. L. Solymar, D. J. Webb, and A. Grunnet-Jepsen, *The Physics and Applications of Photorefractive Materials* (Clarendon, Oxford, 1996).
16. B. I. Sturman, F. Agullo-Lopez, M. Carrascosa, and L. Solymar, "On macroscopic description of photorefractive phenomena," Appl. Phys. B **68**, 1013–1020 (1999).